27th Summer School and International Symposium on the Physics of Ionized Gases (SPIG 2014) IOP Publishing
Journal of Physics: Conference Series **565** (2014) 012008 doi:10.1088/1742-6596/565/1/012008

Resistive Plate Chambers: electron transport and modeling

D Bošnjaković, Z Lj Petrović and S Dujko

Institute of Physics, University of Belgrade, Pregrevica 118, 11070 Belgrade, Serbia

E-mail: dbosnjak@ipb.ac.rs

Abstract. We study the electron transport in gas mixtures used by Resistive Plate Chambers (RPCs) in high energy physics experiments at CERN. Calculations are performed using a multi term theory for solving the Boltzmann equation. We identify the effects induced by non-conservative nature of electron attachment, including attachment heating of electrons and negative differential conductivity (NDC). NDC was observed only in the bulk component of drift velocity. Using our Monte Carlo technique, we calculate the spatially resolved transport properties in order to investigate the origin of these effects. We also present our microscopic approach to modeling of RPCs which is based on Monte Carlo method. Calculated results for a timing RPC show good agreement with an analytical model and experimental data. Different cross section sets for electron scattering in $C_2H_2F_4$ are used for comparison and analysis.

1. Introduction

Resistive Plate Chambers (RPCs) emerged in 1980s as a practical alternative to spark counters with localized discharge [1, 2]. Their reliability comes from electrodes of high resistivity, such as glass or bakelite, which are used to suppress the destructive discharges. Owing to their good efficiency and spatial resolution in conjunction with outstanding timing resolution [3, 4], they are mainly used for timing and triggering in high energy physics experiments [5–7], but they also found their way in other fields such as medical imaging [8, 9] and geophysics [10].

There were many approaches to RPC modeling, mostly analytical [11, 12], fluid [13–15] or Monte Carlo based [16]. The common thread among all these models is that they require electron transport data as input parameters. Electron transport data are usually calculated from the knowledge of cross sections for electrons scattering using Boltzmann equation analysis and/or Monte Carlo technique. A Monte Carlo tool for such a task — MAGBOLTZ [17] has cross sections imbedded in the code and is often used by the particle detector community. The question of reliability was raised in case of cross sections for $C_2H_2F_4$ [18] which is the main component in gas mixtures for RPCs operated in avalanche mode. Another issue is the correct implementation of transport data in RPC modeling when non-conservative collisions such as attachment or ionization are present. In this regard, the duality of transport coefficients is often neglected which in some cases may lead to incorrect results for RPCs performances, i.e. efficiency, timing resolution and charge spectra.

In this paper, we review our recent efforts and outline some of our key results in studying of electron transport and modeling of RPCs. Results are obtained using our multi term theory for solving Boltzmann's equation and Monte Carlo method which are briefly described in Section 2.

In Section 3.1, we investigate the electron transport in RPC gas mixtures used in ALICE, ATLAS and CMS experiment at CERN. Finally, our new microscopic model of RPCs based on Monte Carlo simulation technique is described in Section 3.2. For more details the reader is referred to our recent papers about the electron transport in RPCs [19] and our microscopic approach to RPC modeling [20].

2. Theoretical methods

2.1. Boltzmann equation analysis

Transport coefficients for electrons drifting and diffusing through a background gas under the influence of spatially homogeneous electric field **E**, can be evaluated by solving Boltzmann's equation:

$$\frac{\partial f}{\partial t} + \mathbf{c} \cdot \frac{\partial f}{\partial \mathbf{r}} + \frac{e}{m}\mathbf{E} \cdot \frac{\partial f}{\partial \mathbf{c}} = -J(f, f_0)\,, \tag{1}$$

where $f(\mathbf{r}, \mathbf{c}, t)$ is the phase-space distribution function and e and m are the charge and mass of the electron. $J(f, f_0)$ is the collision integral for electron-gas interactions, including elastic, inelastic and non-conservative (e.g. electron attachment and/or ionization) collisions. f_0 is the Maxwellian velocity distribution function of the neutral gas at $T = 293$ K.

We solve the Boltzmann equation (1) using a numerical technique initially developed by Robson and Ness [21] and later extended by White et al. [22] and Dujko et al. [23, 24]. Among many important aspects, we emphasize the following important steps in solving Boltzmann's equation:

(i) The angular dependence of f is represented in terms of an expansion in spherical harmonics. In contrast to classical two-term theory, our analysis is 'multi term', and we take as many spherical harmonics as are necessary to achieve the full convergence of transport coefficients.

(ii) The speed (energy) dependence of f is represented by an expansion about a Maxwellian at an arbitrary temperature, in terms of Sonine polynomials.

(iii) Transport coefficients are calculated assuming the hydrodynamic conditions. Thus, the spatial dependence of f is treated by the density gradient expansion.

Substitution of these expansions into the Boltzmann equation (1) leads to a hierarchy of coupled differential equations for the moments of f. These equations are numerically solved and all transport coefficients of interest, including the mean energy, drift velocity and diffusion tensor as well as rate coefficients are expressed in terms of these moments [19].

2.2. Monte Carlo simulation technique

Here we outline only the basic concepts behind of our Monte Carlo technique. A thorough description can be found in our recent reviews [25–27].

We assume that the background gas molecules are stationary (zero gas temperature). Each electron is tracked by the analytical solution of the equation of electron motion in electric (and magnetic) field. The moment of collision is determined using the integration method where an electron is moved in very small time steps (compared to collision frequency) while the cumulative probability for a collision is less than a generated random number. When the collision occurs, the type of collision is determined using relative probabilities of different processes determined by the cross sections. The scattering is assumed to be isotropic. In an elastic collision, the electron loses energy of about $2m/M$ where m and M are the electron and molecule mass, respectively. When an inelastic collision or ionization takes place, the electron energy is reduced by the energy loss of that process. After ionization, each division of the remaining energy between the primary and secondary electron is considered to be equally probable. If attachment occurs, the electron is removed from the simulation.

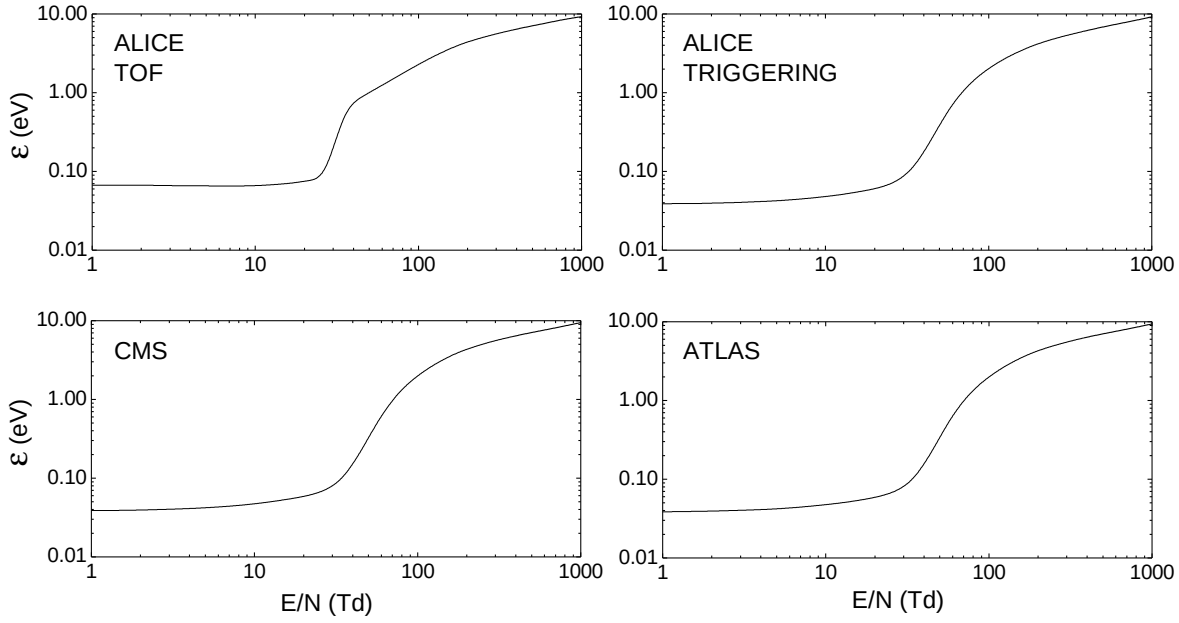

Figure 1. Variation of the mean energy with E/N for RPCs used in ALICE, CMS and ATLAS experiments at CERN. Taken from [19].

Our Monte Carlo technique can also be used to calculate the spatially resolved transport data using the following procedure. First we calculate the mean position (centre of mass) and the standard deviation (σ) of the electron swarm, for each coordinate axis. The interval $(-3\sigma\,, +3\sigma)$ around the mean position is then divided into 100 cells along each axis. Finally, the data including the electron average energy and average velocity, and attachment rate coefficient are calculated for every cell.

3. Results and discussion

3.1. A study of electron transport in RPC gases

First, we present the results for electron transport calculated using Boltzmann equation analysis. The results are calculated for the RPC gas mixtures of $C_2H_2F_4$/iso-C_4H_{10}/SF_6 employed at CERN LHC: (1) ALICE timing (TOF) RPC, 90/5/5; (2) ALICE triggering RPC, 89.7/10/0.3; (3) CMS triggering RPC, 96.2/3.5/0.3; and (4) ATLAS triggering RPC, 94.7/5/0.3. The following is assumed: the cross section set for $C_2H_2F_4$ was developed by our group [28], cross sections for iso-C_4H_{10} are taken from MAGBOLTZ 2.7.1 code and cross sections for SF_6 are taken from Itoh et al. [29]; the temperature and pressure of the background gas is 293 K and 1 atm, respectively; the reduced electric field strength E/N is given in Td (1 Td $= 1 \times 10^{-21}$ Vm^2).

Mean electron energies as a function of E/N are shown in Figure 1. One can observe that the mean energy is nearly constant up to about 30 Td where the energy begins to rise noticeably. This cooling effect is due to rising collision frequency for vibrational excitation of $C_2H_2F_4$. Above 30 Td the cross sections for vibrational excitations begin to drop and therefore the energy increases. Another interesting effect can be observed in case of ALICE TOF mixture with the highest SF_6 content: for lower electric fields, the mean energy is significantly higher than the thermal value of 0.038 eV. This effect is known as *attachment heating* [21] since low energy electrons are consumed in attachment and consequently the mean energy increases.

Figure 2 shows the calculated drift velocities. In case of ALICE TOF mixture, bulk component

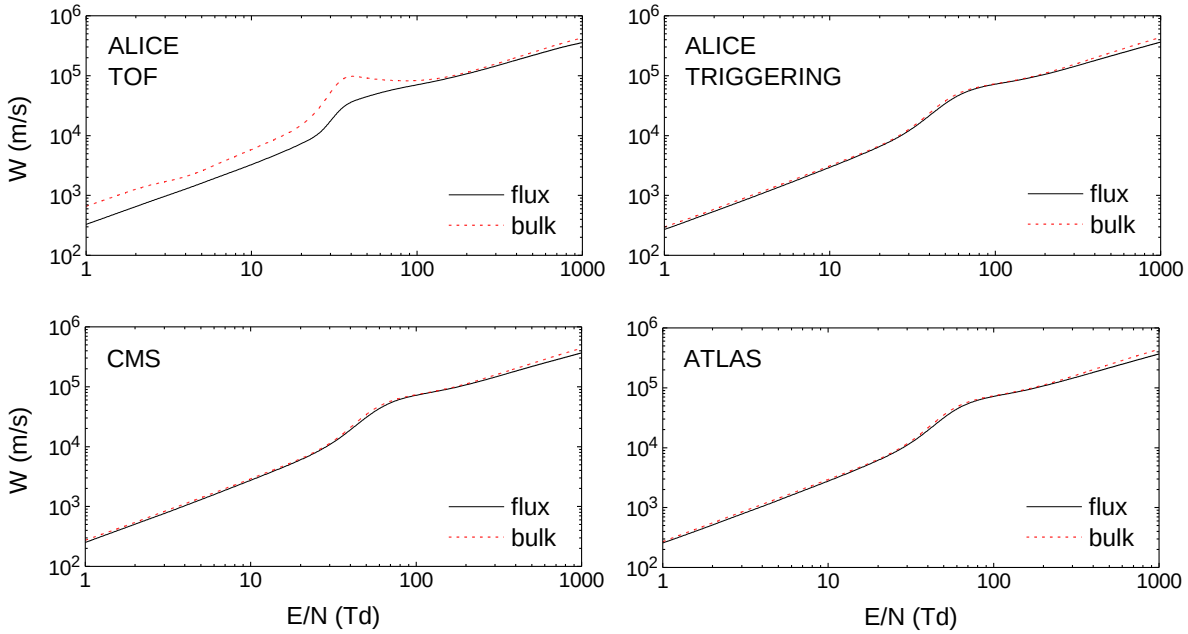

Figure 2. Variation of the bulk and flux drift velocities with E/N for RPCs used in ALICE, CMS and ATLAS experiments at CERN. Taken from [19].

of drift velocity exhibits a strong negative differential conductivity (NDC). NDC is a kinetic phenomenon defined as a decrease of drift velocity with increasing electric field [30]. It can arise due to a certain combination of elastic and inelastic cross sections and is usually present in both flux and bulk components of drift velocity. In this case however, the NDC is only present in the bulk drift velocity and the question of whether this is possible was already raised [31]. The effect can be understood by analyzing the spatial profiles of the electron swarm. For that purpose we use our Monte Carlo method to calculate the spatially resolved data including the mean energy and attachment rate coefficient. The Monte Carlo calculations are performed using cold gas approximation ($T = 0$) and therefore the calculated values are shifted with respect to those obtained using Boltzmann equation. Figure 3a shows the spatial profile and mean energy along the swarm for $E/N = 10$ Td which corresponds to the peak of bulk drift velocity (the onset of NDC). It can be seen that the mean energy is not constant along the swarm. Electrons at front of the swarm have more energy than those at the back and thus the attachment rate is higher at the back than at the front having in mind the energy dependence of cross section for attachment. As a consequence, the center of mass of the swarm shifts forward which is observed as an increase of bulk drift velocity over the flux component. The difference between flux and bulk component is roughly proportional to the spatial gradient of the attachment rate coefficient (Figure 3b). Indeed, one can see that the highest gradient corresponds to the peak of bulk drift velocity for $E/N = 10$ Td. As electric field increases, the gradient drops and the NDC gradually diminishes.

3.2. Our Monte Carlo model of RPCs

In this section, we present the results for timing distributions of electron avalanches and also the performance characteristics of a timing RPC with a gas mixture of 85% $C_2H_2F_4$ + 5% iso-C_4H_{10} + 10% SF_6. Results are calculated using our Monte Carlo method described in Section 2.2.

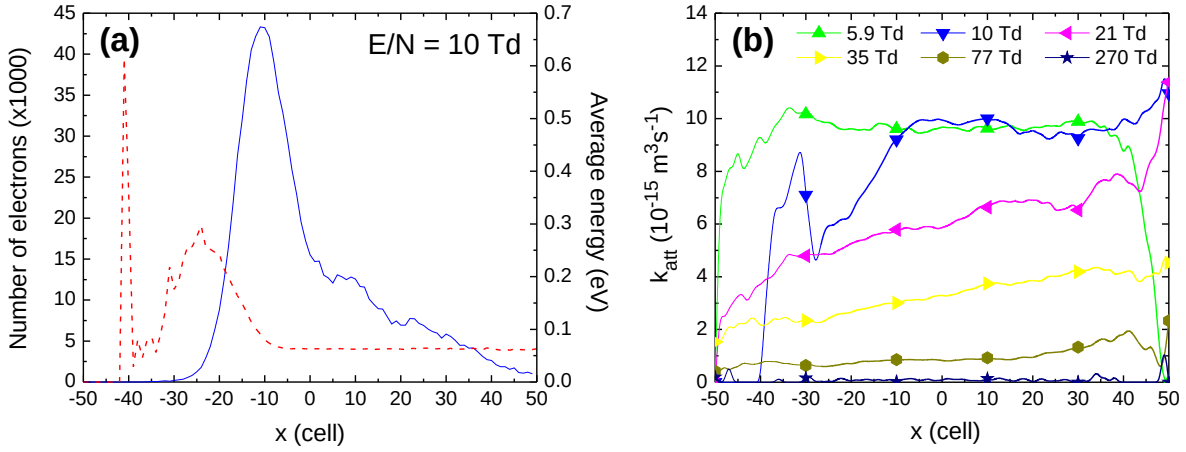

Figure 3. Spatially resolved transport properties for ALICE timing RPC gas mixture ($t = 1$ ns). The x axis is in the direction of the electric field. (a) Spatial profile of electrons (solid line) and spatially resolved averaged energy (dashed line) at $E/N = 10$ Td. (b) Spatially resolved attachment rate coefficient for a range of E/N. Taken from [19].

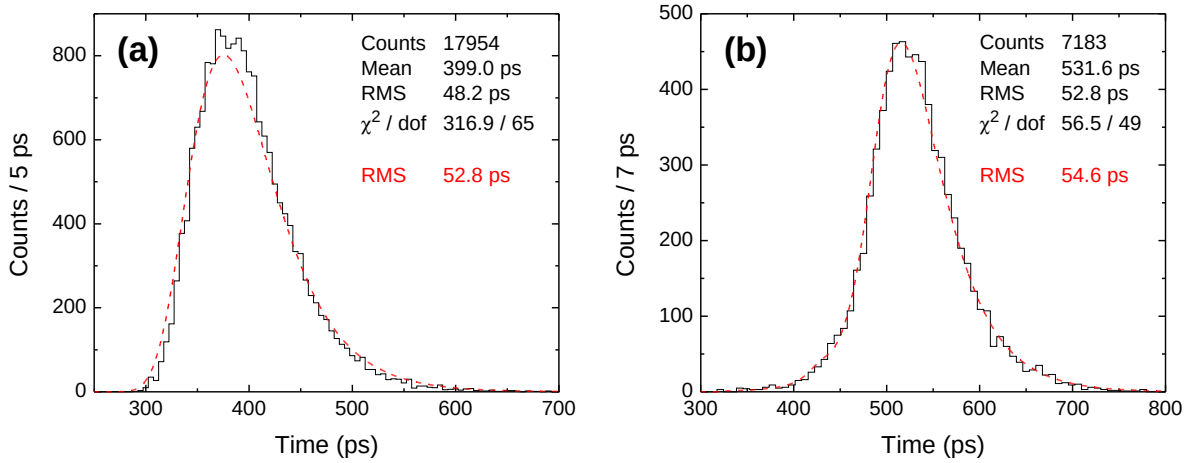

Figure 4. Timing distributions compared to analytical model [11] (dashed lines) for $E/N = 439$ Td. Our cross sections for $C_2H_2F_4$ [28] are assumed. (a) Single electron avalanches: the threshold is set to 10000 electrons. (b) Realistic RPC events: electron avalanches started by primary ionization generated using HEED cluster size distribution; gas gap 0.3 mm; the threshold is set to 2 fC. Taken from [20].

Cross sections for electron scattering are the same as in Section 3.1.

Figure 4a shows the timing distribution for single electron avalanches in an infinite space. The distribution agrees well with an analytical model [11]. This analytical model is based on Legler's model [32] of avalanche fluctuations and thus the slight difference between the timing distributions can be attributed to the approximation of constant probability for an ionization which is assumed by Legler's model.

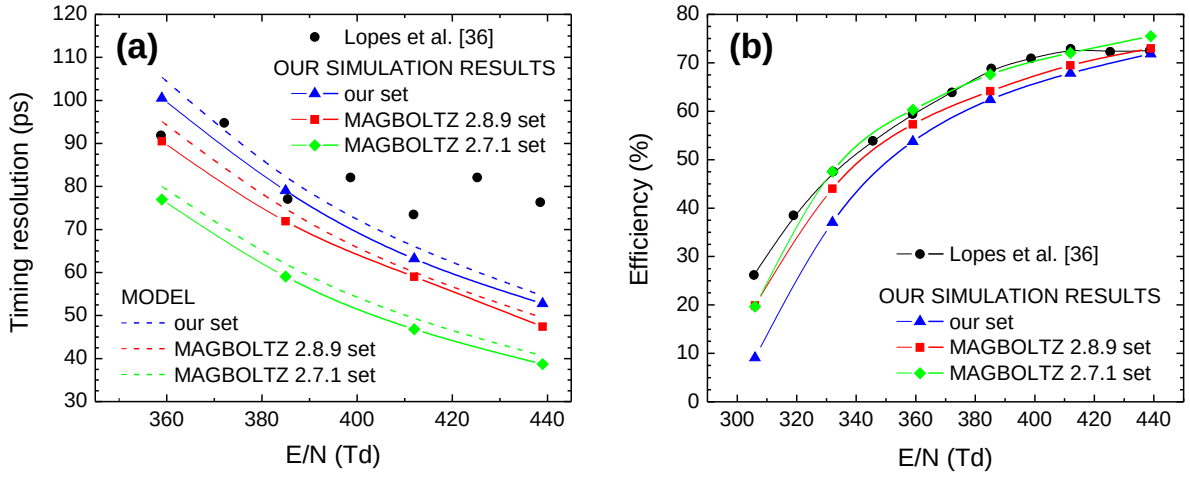

Figure 5. (a) Timing resolutions and (b) efficiencies calculated for a specific timing RPC using different $C_2H_2F_4$ cross section sets and HEED cluster size distribution. Comparison with experimental values by Lopes et al. [36] and analytical model [11] (dashed lines). Taken from [20].

The realistic RPC model, in addition to electron avalanche fluctuations, includes the effects of primary ionization, boundaries (i.e. gas gap) and the threshold given by induced charge. Primary ionization is implemented using a simple model which assumes that the primary electrons are grouped in clusters while the distance between the neighboring clusters follows the exponential distribution. Mean distance between the clusters and cluster size distribution are calculated using HEED [33] assuming minimum ionizing particles. The boundaries are determined by the 0.3 mm gas gap with "absorbing" anode. The threshold is set to 2 fC of induced charge which corresponds to about 10^6 electrons in the gas gap. The induced charge is calculated as an integral of the induced current which is given by Ramo's theorem [34].

A timing distribution calculated using the described RPC model is shown on Figure 4b. The distribution has a typical Gaussian-like shape. The left tail of the distribution represents the fastest events which most probably come from large primary ionization while the right tail is mainly determined by the electron avalanche fluctuations.

Finally, we show the results for the timing resolution and detection efficiency. For comparison, the results are made using different cross sections sets for $C_2H_2F_4$. In addition to our set, we use a set from MAGBOLTZ 2.8.9 (which is updated concerning the latest measurements [35]) and the older version from MAGBOLTZ 2.7.1. The timing resolution (Figure 5a) and detection efficiency (Figure 5b) both noticeably depend on the cross sections used. The experimentally measured values [36] are also shown for comparison.

4. Conclusion

We have presented some of our recent results in studying of electron transport in RPC gases and modeling of RPCs. Studies of electron transport reveal some interesting phenomena, induced by the explicit and implicit effects of electron attachment. In particular, the NDC effect is present only in the bulk component of drift velocity while unusually strong attachment heating is observed in the profile of the electron mean energy. Both of these phenomena are observed in case of ALICE TOF gas mixture. Using our Monte Carlo technique to evaluate the spatial profiles of the electron swarm we are able to illustrate and prove that the NDC is induced by strong attachment due to higher concentration of SF_6. In addition, our microscopic approach to

RPC modeling shows how to calculate the RPC performance characteristic of a timing RPC by following the individual electrons in a Monte Carlo fashion. The results for timing distributions agree well with an analytical model which uses the approximation of constant probability for ionization. The calculated timing resolution and efficiency agree well with experimental data and they also show sensitivity with respect to cross section sets for electron scattering used for $C_2H_2F_4$.

Acknowledgments

This work is supported by MPNTRRS Projects OI171037 and III41011.

References

[1] Santonico R and Cardarelli R 1981 *Nucl. Instrum. Meth.* **187** 377–380
[2] Cardarelli R, Santonico R, Di Biagio A and Lucci A 1988 *Nucl. Instrum. Meth. A* **263** 20–25
[3] Santonico R 2012 *Nucl. Instrum. Meth. A* **661** S2–S5
[4] Fonte P 2002 *IEEE Trans. Nucl. Sci.* **49** 881–887
[5] The ATLAS Collaboration 2008 *J. Instrum.* **3** S08003
[6] The ALICE Collaboration 2008 *J. Instrum.* **3** S08002
[7] The CMS Collaboration 2008 *J. Instrum.* **3** S08004
[8] Blanco A, Couceiro M, Crespo P, Ferreira N C, Ferreira Marques R, Fonte P, Lopes L and Neves J A 2009 *Nucl. Instrum. Meth. A* **602** 780–783
[9] Couceiro M, Crespo P, Mendes L, Ferreira N, Ferreira Marques R and Fonte P 2012 *Nucl. Instrum. Meth. A* **661** S156–S158
[10] Cârloganu C, Niess V, Béné S, Busato E, Dupieux P, Fehr F, Gay P, Miallier D, Vulpescu B, Boivin P, Combaret C, Labazuy P, Laktineh I, Lénat J-F, Mirabito L and Portal A 2013 *Geosci. Instrum. Method. Data Syst.* **2** 55–60
[11] Riegler W 2009 *Nucl. Instrum. Meth. A* **602** 377–390
[12] Mangiarotti A, Fonte P and Gobbi A 2004 *Nucl. Instrum. Meth. A* **533** 16–21
[13] Khosravi Khorashad L, Moshaii A and Hosseini S 2011 *EPL (Europhys. Lett.)* **96** 45002
[14] Khosravi Khorashad L, Eskandari M and Moshaii A 2011 *Nucl. Instrum. Meth. A* **628** 470–473
[15] Moshaii A, Khosravi Khorashad L, Eskandari M and Hosseini S 2012 *Nucl. Instrum. Meth. A* **661** S168–S171
[16] Riegler W and Lippmann C 2004 *Nucl. Instrum. Meth. A* **518** 86–90
[17] Biagi S F 1999 *Nucl. Instrum. Meth. A* **421** 234–240
[18] Gonzalez-Diaz D and Sharma A 2012 Current Challenges and Perspectives in Resistive Gaseous Detectors: a manifesto from RPC 2012 *in proceedings of the "XI workshop on Resistive Plate Chambers and Related Detectors (RPC2012)", PoS (RPC2012) 084*
[19] Bošnjaković D, Petrović Z Lj, White R D and Dujko S 2014 *J. Phys. D: Appl. Phys.* **47** 435203
[20] Bošnjaković D, Petrović Z Lj and Dujko S 2014 *J. Instrum.* **9** P09012
[21] Robson R E and Ness K F 1986 *Phys. Rev. A* **33** 2068–2077
[22] White R D, Robson R E, Dujko S, Nicoletopoulos P and Li B 2009 *J. Phys. D: Appl. Phys.* **42** 194001
[23] Dujko S, White R D, Petrović Z Lj and Robson R E 2010 *Phys. Rev. E* **81** 046403
[24] Dujko S, White R D, Petrović Z Lj and Robson R E 2011 *Plasma Sources Sci. Technol.* **20** 024013
[25] Dujko S, Raspopović Z M and Petrović Z Lj 2005 *J. Phys. D: Appl. Phys.* **38** 2952–2966
[26] Dujko S, White R D, Ness K F, Petrović Z Lj and Robson R E 2006 *J. Phys. D: Appl. Phys.* **39** 4788–4798
[27] Dujko S, White R D and Petrović Z Lj 2008 *J. Phys. D: Appl. Phys.* **41** 245205
[28] Šašić O, Dupljanin S, de Urquijo J and Petrović Z Lj 2013 *J. Phys. D: Appl. Phys.* **46** 325201
[29] Itoh H, Matsumura T, Satoh K, Date H, Nakao Y and Tagashira H 1993 *J. Phys. D: Appl. Phys.* **26** 1975–1979
[30] Petrović Z Lj, Crompton R W and Haddad G N 1984 *Aust. J. Phys.* **37** 23
[31] Vrhovac S B and Petrović Z Lj 1996 *Phys. Rev. E* **53** 4012–4025
[32] Legler W 1961 *Z. Naturforsch.* **16a** 253
[33] Smirnov I 2005 *Nucl. Instrum. Meth. A* **554** 474–493
[34] Ramo S 1939 *Proc. I.R.E.* **27** 584
[35] de Urquijo J, Juárez A M, Basurto E and Hernández-Ávila J L 2009 *Eur. Phys. J. D* **51** 241–246
[36] Lopes L, Fonte P and Mangiarotti A 2012 *Nucl. Instrum. Meth. A* **661** S194–S197